Title: **Fretting fatigue tests on shrink-fit specimens and investigations into the strength enhancement induced by deep rolling**

Authors: **L. Bertini, C. Santus**

DOI Link: https://doi.org/10.1016/j.ijfatigue.2015.08.007

Fretting fatigue tests on shrink-fit specimens and investigations into the strength enhancement induced by deep rolling

L. Bertini[a], C. Santus[a,*]

[a]*University of Pisa. DICI - Department of Civil and Industrial Engineering. Largo L. Lazzarino 2, 56122 Pisa, Italy.*

Abstract

The shrink-fit connection undergoes fretting fatigue at the edge of the contact, where both stress concentration and micro-slip take place. A fretting test set-up with a round-shaped specimen is proposed that eliminates lateral edge contact and misalignment, and is also appropriate for deep rolling. Comparative experiments showed a notable strength improvement, induced by deep rolling, along with the beneficial effect of friction reduction due to lubrication. Multiple cracks with clear shallow paths were evident after SEM observation, thus the maximum shear stress amplitude was assumed as a correlating parameter, while the crack arrest was inappropriate especially for deep rolled specimens.

Keywords: Fretting fatigue; Fretting test setup; Deep rolling; Residual stresses; 7075-T6 aluminium alloy.

*Corresponding author: Ciro Santus
Ph. +39 (0)50 2218007, Fax +39 (0)50 2210604.
Email address: ciro.santus@ing.unipi.it (C. Santus)

Nomenclature

SIF	Stress Intensity Factor.
FE	Finite Element (model).
SEM	Scanning Electron Microscope.
KT	Kitagawa-Takahashi (diagram).
CoF	Coefficient of Friction.
f	CoF value.
R_a	Surface average roughness.
σ_a	Bending stress amplitude.
N_f	Number of cycles to failure.
E	Young's modulus.
ν	Poisson's ratio.
σ_{ij}	Stress components for the singularity problem.
r	Radial coordinate for stress singularities.
m	Order of singularity.
p	Pressure distribution at the fretting interface.
s	Shear traction at the fretting interface.
R	Fatigue load cycle ratio.
$K_\mathrm{I}, K_\mathrm{II}$	Mode I and mode II SIFs.
$\Delta K_\mathrm{I,p}$	Positive (or tensile) part of the mode I SIF range.
ΔK_II	Mode II SIF range.
α	Crack direction angle, also used for critical plane orientation.
$\Delta K_{\mathrm{th},-1}$	Threshold SIF range, $R=-1$.
$\Delta\sigma_{-1}$	Fatigue limit (or fatigue endurance) stress range, $R=-1$.
L	El Haddad length evaluated for $R=-1$.

$\Delta K_{\mathrm{th,0}}$	Threshold SIF range, $R = 0$.
$\Delta K_{\mathrm{th,0,Asy}}$	Short crack threshold SIF range, asymptotic model, $R = 0$.
$\Delta K_{\mathrm{th,0,EH}}$	Short crack threshold SIF range, El Haddad model, $R = 0$.
τ_{a}	Shear stress amplitude.
$\sigma_{\mathrm{n,max}}$	Maximum normal stress.
$\sigma_{\mathrm{n,min}}$	Minimum normal stress.
$\sigma_{\mathrm{n,a}}$	Normal stress amplitude.
κ, λ	Multiaxial fatigue material parameters.
κ_i, λ_i	Multiaxial parameters obtained by combining different load ratios.
$\tau_{\mathrm{a,eq}}$	Equivalent multiaxial fatigue shear stress amplitude.
η	Multiaxial criterion assessment stress ratio.

1. Introduction

Mechanical components with a highly loaded contact and local micro-slippage can undergo fretting fatigue. Examples of fretting fatigue include the dovetail interface of turbomachinery [1, 2, 3, 4] and the shrink-fit (tubular or cylindrical) connection [5, 6, 7, 8, 9, 10, 11]. Fretting testing is essential in designing admissible loads and also to validate different modelling approaches. Experimental fretting tests can be classified into: (1) full or small scale replication of the actual fretting configuration, as experienced by the in-service component, and (2) idealized test layout where the contact is accurately controlled [12, 13]. Examples of component testing have been presented by Golden et al. [4, 14] regarding the dovetail interface, by Bertini et al. [9] and Alfredsson [10] regarding shrink-fit connection, and Azevedo et al. [15] regarding cable clamping, as well as others for different applications. Controlled contact fretting tests are well summarized in Hills and Nowell [12], and the usual layout is the "bridge" type with a two sided contact pad. Many examples of this kind of testing have been reported in the literature, such as the books by Attia and Waterhouse [16], Hoeppner et al. [17] and Mutoh et al. [18]. The main limitation of bridge type testing is that the displacement can never be the same on the two sides of the contact pad, thus leading to dissimilar fretting configurations, though nominally equal [12]. This problem can be solved after fixing one side of the contact bridge to the rigid part of the testing frame. This solution has been reported by McVeigh et al. [1], Rossino et al. [19], Araújo et al. [20], Lykins et al. [21, 22], Szolwinski and Farris [23], and others. The contact configuration of bridge type testing may be Hertzian, cylindrical to flat [24, 25, 23], or even sphere to flat [26], while sharp complete contacts without rounded corners have recently been proposed by Hojjati-Talemi et al. [27], Giner et al. [28] and Noraphaiphipaksa et al. [29]. Although the "flat and rounded" contact is common for dovetail joints, only a few examples are available in the literature, such as McVeigh [1] et al. and Namjoshi et al. [30]. Despite the simplicity of bridge testing, two further problems need to be considered: the lateral edge contact and the tilt. The lateral edge contact effect was investigated by Kim and Mall [31], who correctly analysed plane strain at the centre and plane stress at the sides. Of these two cases, the plane stress should be the less critical provided that a precise lateral alignment is ensured, which otherwise would load to an edge stress singularity. A potential solution was proposed by Liu and Hill [32] who introduced rounded lateral edges which led to a non-singular boundary stress distribution. Preventing any angle misalignment between the specimen and the pad also needs to be considered. This issue can induce a non uniform pressure along the transversal direction, as shown by Kim and Mall [31] and also discussed by Wittkowsky et al. [26]. In addition, the flat either rounded or not rounded contact, may tilt during the load cycle, thus producing a non-optimal contact fluctuation [33]. The fretting test layout proposed in this paper is based on a round geometry with a small conical angle, for shrink-fitting, and loaded by cyclic bending. This contact

configuration does not involve an edge effect nor misalignment, however, the bending causes a contact pressure oscillation during the load cycle (resembling the tilting issue) but thoroughly taken into account by means of a finite element model. This testing layout is both aimed at an accurate contact load configuration, and also reproduces a shrink-fit connection, thus the obtained results can even be rescaled to actual components.

The modelling approaches to fretting fatigue are summarized by Nowell et al. [34], Hills et al. [35] and are: analogies either with crack or notch, Ciavarella [36, 37, 38] and Naboulsi [39]; asymptotic approaches both for complete and incomplete contacts, Dini, Nowell, Hills et al. [34, 35, 40, 41, 42, 43]; short crack arrest on the Kitagawa-Takahashi (KT) diagram, Araújo et al. [19, 20, 44] and Vallelano et al. [45]; and finally a multiaxial fatigue critical plane approach, usually associated with a material size in order to incorporate the gradient effect, Araújo et al. [19, 20, 46]. Of these approaches, crack arrest implicitly assumes that fretting is a *tensile* driven fatigue mechanism, indeed the reference threshold Stress Intensity Factor (SIF) is according to the mode I, which is the opening mode. The aim of the present paper is to show comparative results and assess the effect of the deep rolling surface treatment, which induces highly compressive residual stresses. As shown later, the crack opening is completely prevented, after deep rolling, thus the crack arrest criterion is questionable for these fretting tests since the first stage of fatigue propagation is no longer driven by mode I loading. A multiaxial fatigue critical plane approach, based on the shear stress amplitude, is expected to be more suitable. The consistency of the predictive model can also be tested on the basis of the crack propagation direction, especially by taking into account the early stages of the crack. The initial crack orientation in fretting fatigue is broadly discussed in the literature. The papers by Lamacq and Dubourg [17, 47] distinguished type I and type II cracks as initially shallow, rather than almost perpendicular to the surface, and they were clearly attributed to shear and normal tensile stresses, respectively. The vertical orientation of the initial crack, without a shallow preliminary stage (type II) was observed by Giner et al. [28], Muñoz et al. [24] and also Mutoh et al. [17, 18, 48] who supported the maximum tangential stress criterion, for identifying the direction, even at the very early stage of the crack. In contrast, the present paper shows very shallow cracks with the shear playing a predominant role with respect to the tensile stress.

The present paper includes both experimental and modelling topics. Initially, a new design test geometry is outlined, which is dedicated to the shrink-fit application, either featuring flat and rounded contact or possibly with sharp complete contact. Next, the effects of lubrication and the deep rolling on improving the fretting fatigue strength are investigated. Finally, the modelling of the nucleation process is reported, comparing and discussing various approaches where SEM investigation has been essential for identifying the initial orientation of the crack.

2. Experimental activity

2.1. Fretting fatigue test setup

The proposed experimental setup is shown in Fig. 1. The two fretting parts are the shaft, which is the specimen, and the hub, which plays the role of the fretting pad. As in the configuration proposed by Juoksukangas et al. [49], the cyclic bulk stress was generated by bending instead of axial loading. The bending load was generated by a hydraulic actuator and was fully reversed for all the tests performed. The rear flat surface of the hub was bolted to the mounting parts of the testing frame, and a cantilever scheme was thus obtained. The working frequency of the test was 10 Hz and it was basically limited by the relatively large stroke due to the cantilever compliance. By checking the two extreme values of the actuator displacement, approaching the end of the test, it was possible to identify which side the crack had been propagated to (Fig. 1). The remaining ligament was finally broken after having stopped the test. The recorded number of cycles to failure includes both nucleation and propagation up to a crack size of approximately half the specimen cross section.

As mentioned in the Introduction, the usual configuration with a flat specimen and a lateral contact pad can undergo an edge effect and misalignments. The round shape however, has no edge and mount tilting is prevented by the cylindrical mating of the contacting surfaces. Another advantage of the axisymmetric shape was the easy application of the deep rolling treatment on the shaft specimen. The small conical angle of the two mating parts means that the contact pressure preload can be fine tuned with an adjusting nut which was wrenched during the shrink-fit operation. In principle, the hub acts as a bridge pad, constrained on one side, hence the contact edge of the other side is the fretting point. This is referred to as the "hot-spot", meaning the tangency point between the flat and the fillet profile on the hub side and the mating point on the specimen which experiences the fretting damage. Two strain gages were applied to the two components for load monitoring (Fig. 1). The strain gage on the hub was aligned according to the hoop direction and controlled the shrink-fit operation. The other strain gage was applied along the specimen axis and measured the bending load induced by the actuator. This bending strain gage was at some distance from the fretting hot-spot to prevent any stress concentration effect on the measurement. The stress at the fretting hot-spot was then easily derived by considering the cantilever beam bending distribution. The force produced by the actuator, and measured by a load cell at the actuator head, was in agreement with the bending strain gage reading. Of the two measures, the strain gage was assumed to be more accurate since it was not affected by any dynamic issue which, on the other hand, affect the actuator load cell.

The fretting edge was manufactured with a 2 mm fillet radius. To date, no test has been performed with a sharp edge, however, this interesting fretting case could obviously also be tested with the proposed setup. The shaft specimens were manufactured in aluminium alloy 7075-T6, while the hub was in steel. The hub internal surface

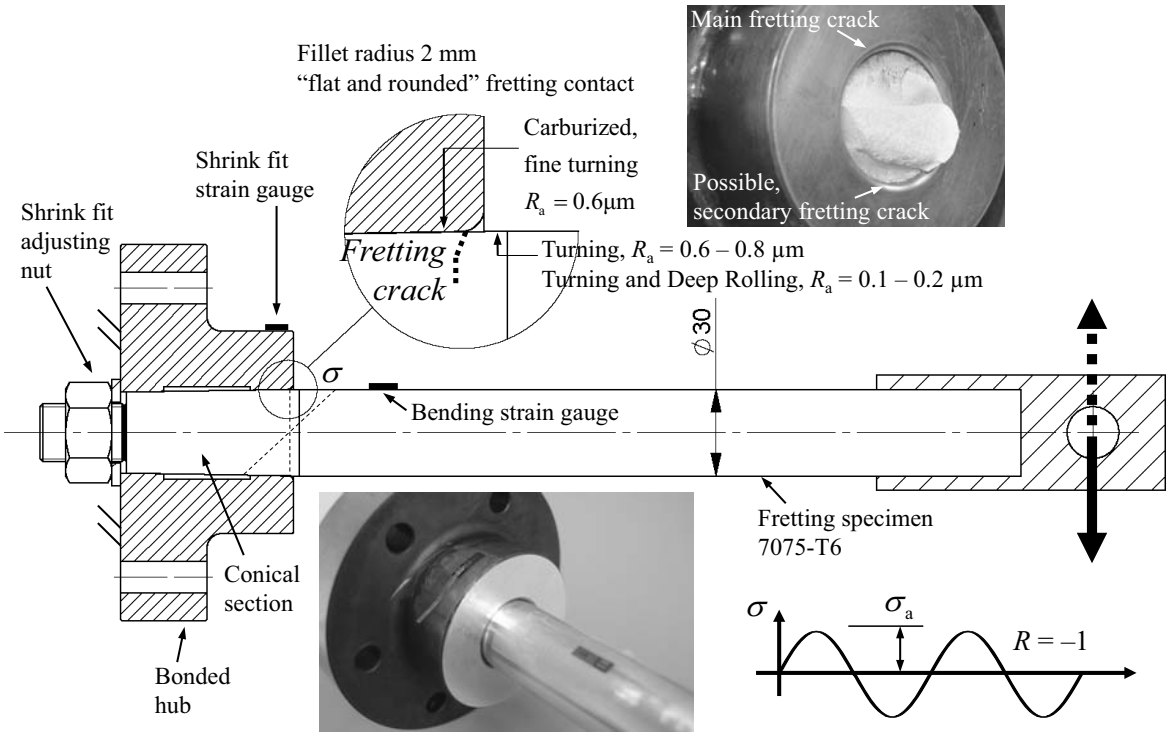

Figure 1: Proposed experimental setup for fretting fatigue on shrink-fit specimens.

was turned, carburized for a notably higher surface hardness than the mating aluminium, and again turned as finishing to gain a very limited surface roughness and accurate shape. Grinding was avoided because the fillet geometry was obtained by imposing a continuous machining profile, on a numerical control turning machine, without dents or other irregularities at the fretting point. The final surface quality was then verified as being similar to a grinding finishing. The shaft conical section was also fine turned and a similar grinding finishing was again obtained $R_a = 0.6 - 0.8$ μm. This surface roughness was also significantly reduced (approximately by a factor of five) after the deep rolling treatment.

2.2. Deep rolling

It is well known that fatigue strength is improved by mechanical treatments that induce surface hardening and residual stresses. Shot peening is the most widely investigated. For example, Benedetti et al. [50] show the enhancement effect produced on the aluminium alloy 7075-T651. Similarly, deep rolling introduces a compressive treatment on the surface, and in the literature fatigue improvement particularly concerns the low plasticity burnishing with the ball type indenter; for example the paper by Prevéy and Cammett on 7075-T6 alloy [51]. Fretting fatigue improvement with shot peened and deep rolling was reported by Majzoobi et al. [52, 53, 54] where a dedicated equipment was used for the rolling of the specimens. Santus et al. [55] recently investigated a conical indenter that can be used both on milling and turning machines, and the parametric dependences of the

residual stress distributions were experimentally obtained. The compressive depth was primarily related to the rolling force, while the rolling feed had an effect on the surface residual stresses and the work hardening. The deep rolling for this fretting activity was performed with the same conical and rounded tool, Fig. 2 (a). After selecting the parameter combination: rolling force 150 N and rolling feed 0.1 mm, the residual stress distribution of Fig. 2 (b) was obtained, with an optimal trade-off with compressive depth, high compressive stress at the surface, and non-excessive plastic deformation. The maximum compressive residual stress was found to be almost as high as the material yield strength, thus producing the highest possible closure effect on a potential fatigue crack. The compressive depth was a few tenths of a millimetre, thus significantly thicker than a shot peening, and larger than the "process zone" which can be assumed to be the same size as the material critical length [56]. Deep rolling also generated a surface finish enhancement, as mentioned above, which may improve the fretting contact since the actual pressure distribution is evened out, however, only the residual stress effect was taken into account for predictive modelling.

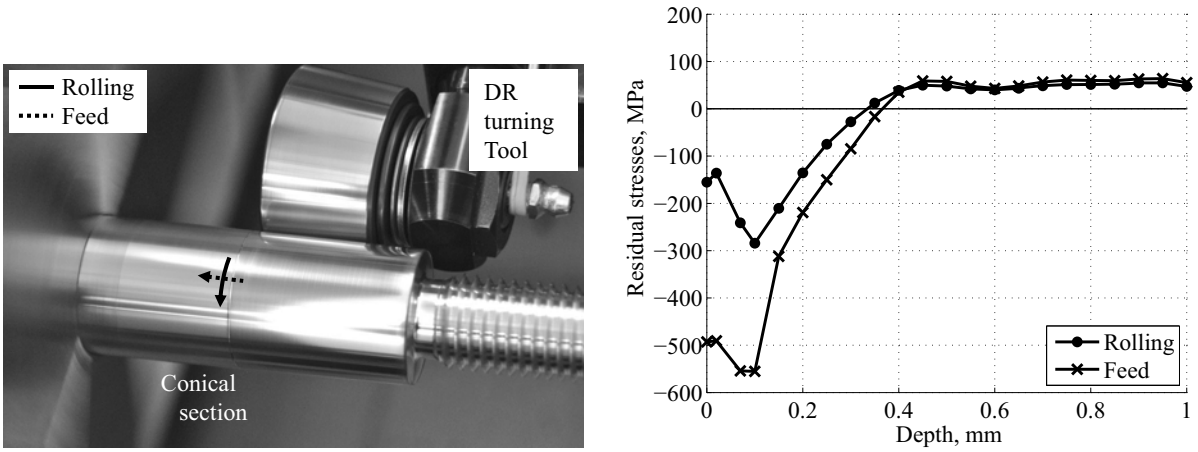

(a) (b)

Figure 2: (a) Deep rolling of the fretting specimen shaft with a conical and rounded tool. (b) Residual stresses along the principal directions.

2.3. Test results

The usual strength enhancement solutions for fretting fatigue consist in introducing of a compressive layer and reducing the coefficient of friction (CoF) [57, 58]. This paper investigates both these solutions. Four series were tested combining deep rolling and the application of a lubricant at the fretting interface before the shrink-fit. Fretting S-N curves are reported in Fig. 3 where the amplitude σ_a refers to the bending stress, evaluated from the beam theory at the fretting hot-spot. The comparative trends are evident, the deep rolling notably increased the fretting strength, as did the introduction of the lubricant. The combination of the two solutions: deep rolling and lubrication, obviously produced the highest strength. These trends are in agreement with the literature

results, for example Lindley [59] reported similar strength improvements produced by both solid lubrication and (shot peening) compressive residual stresses. The use of a solid lubricant is recommended for fretting [60], however, the liquid lubrication was quite effective for the untreated specimens reported here, while producing a limited effect for deep rolled specimens. Indeed, the durability of the lubricant at the fretting interface may have been limited due to the higher load experienced by the deep rolled specimens and, consequently the results of the two series C and D were quite similar. Some of the deep rolled specimens failed at the edge of the rolling treatment, instead of at the fretting hot-spot (hollow dots of Fig. 3), thus proving that the sensitivity to fretting had been overcome by deep rolling.

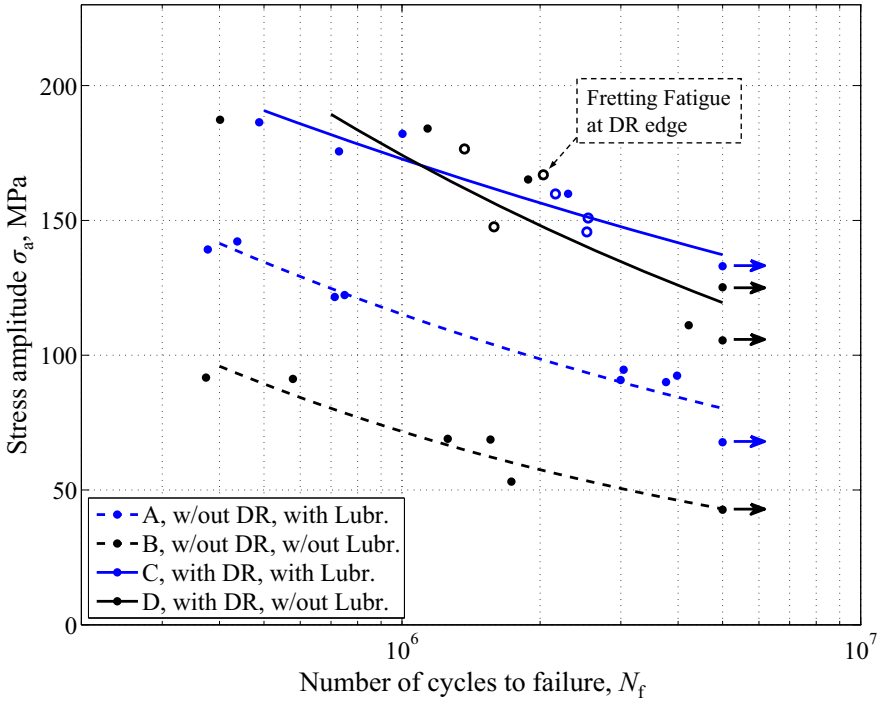

Figure 3: Fretting fatigue results for the test series combinations of deep rolling and lubrication.

The upper part of Fig. 1 shows the fracture section. Only a single fatigue crack was usually observed, and the final fracture obtained after advanced propagation. This predominant crack was either on the upper bending side, or on the lower, indeed the two sides experienced nominally equal stress cycling. Only a few specimens showed significant propagation on both sides, however, one crack was eventually predominant over the other.

2.4. SEM investigation

The detection of the early stages of the fretting cracks was performed on unbroken specimens (runouts) that were cut along the bending axial plane, polished, and then examined with a scanning electron microscope (SEM). Fretting cracks are shown in Fig. 4 for all four series. The first evidence was that multiple cracks, rather than a single predominant crack, were likely to occur especially for the highly loaded C and D series. Crack

Specimen series	A	B	C	D
Slip length, mm	1.5	1.4	5.6	4.5
Slip range, μm	1.1	1.3	8.3	5.9
CoF, f	0.37	0.51	0.51	0.55

Table 1: Deduced values of the coefficient of friction for the test series.

coalescence and branching were also evident on these deep rolled specimens. The material was also abraded for the C series at the edge contact, while it piled up for non-lubricated B and D series specimens. The direction of the initial cracking was mainly focused. All the sections reported a pattern with shallow cracks. As previously mentioned, these observed cracks can be classified as type I [47] however, regarding series A, C and D, further propagation still remains with a shallow angle for relatively large crack lengths. Only series B showed a slight direction change approximately at a crack length of 10 μm, still with a very shallow initiation. Subsequently, the crack propagation became perpendicular to the axis of the specimen for larger crack sizes, in the order of 1 mm, which is outside the scope of Fig. 4.

2.5. Coefficient of friction

Accurately assessing the CoF is crucial for predicting fretting stresses. The overloading technique, as proposed in the literature, can be used along with displacement measuring [26, 61, 62]. This kind of testing was not possible with the present fretting geometry, however, a different technique was used and the steel to aluminium CoF was found under the specific conditions of lubrication and surface finish. The surfaces of the specimens were scanned with a profilometer at the end of the test, after disengaging the shaft with the hub. The slippage length was evaluated from the change in surface morphology (Fig. 5). Finite element (FE) modelling, introduced below, easily returned the slippage length and this distance was clearly dependent on both the load and the CoF numerical value f inputted into the model. After tuning f the experimental slip length was matched to the finite element simulation. The CoF values are reported in Table 1, which also shows the slip range for each specimen that was used for finding the CoF. As mentioned above, lubrication was most effective for the non deep rolled series A that experienced lower fretting. On the other hand, similar values were obtained for the deep rolled two series, approximately $f = 0.5$. Although the generic steel to aluminium CoF is usually smaller for dry contact ($f = 0.3$, Santus et al. [63]) the *fretting* CoF values were found to be higher, in the range $0.6 - 0.75$, especially after a significant portion of the fretting life [61]. Furthermore, high fretting CoF is usual with the same material for the two mating parts, while the contacting metals are different in the present investigation.

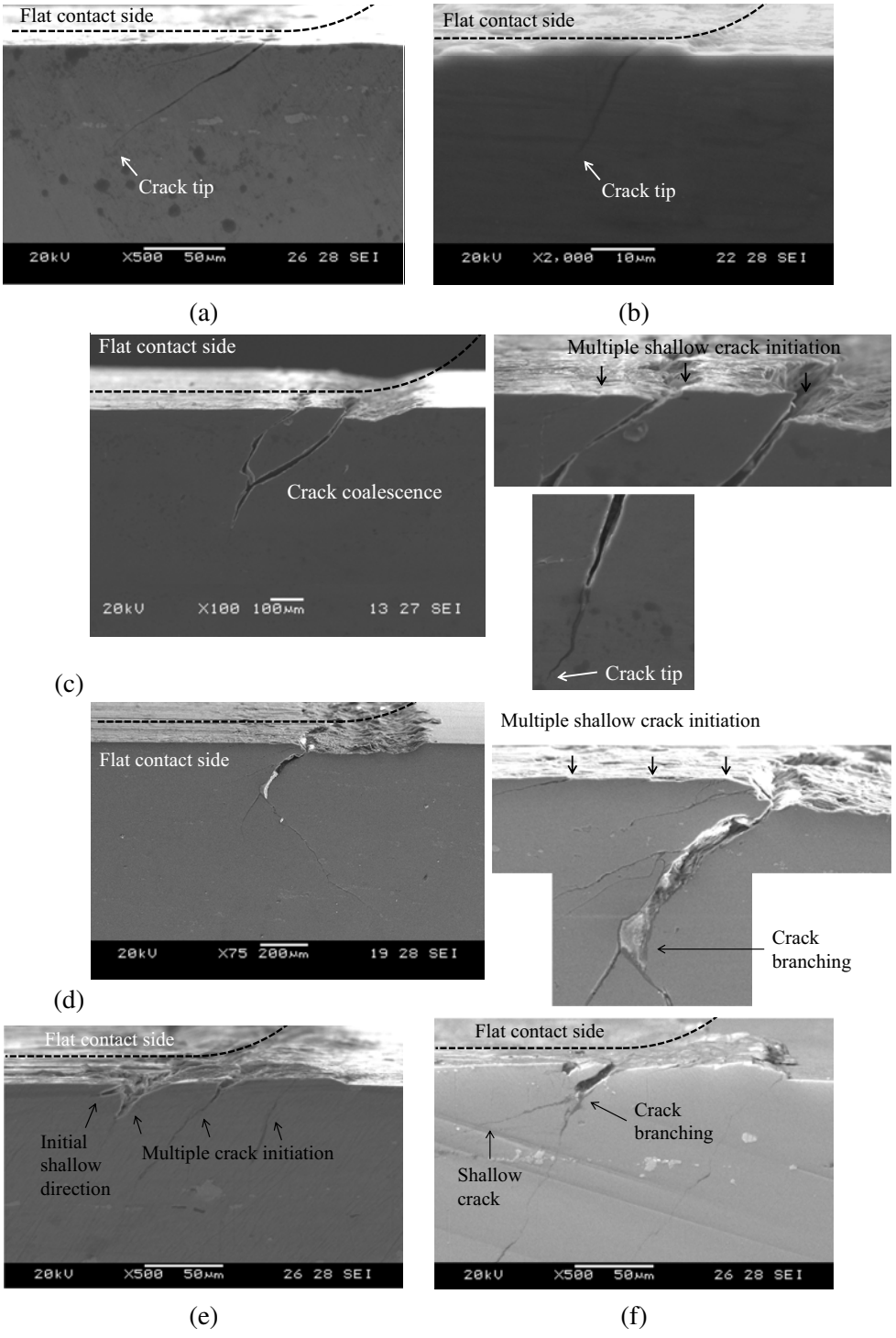

Figure 4: SEM section observations: (a) and (b) w/out deep rolling, A and B series respectively, (c), (d) C series and (e), (f) D series.

3. Numerical analyses

3.1. FE model

The specific geometry of this axisymmetric fretting assembly did not require any cumbersome three-dimensional FE simulation. The submodelling produced accurate simulations with a limited calculation time. Initially, two

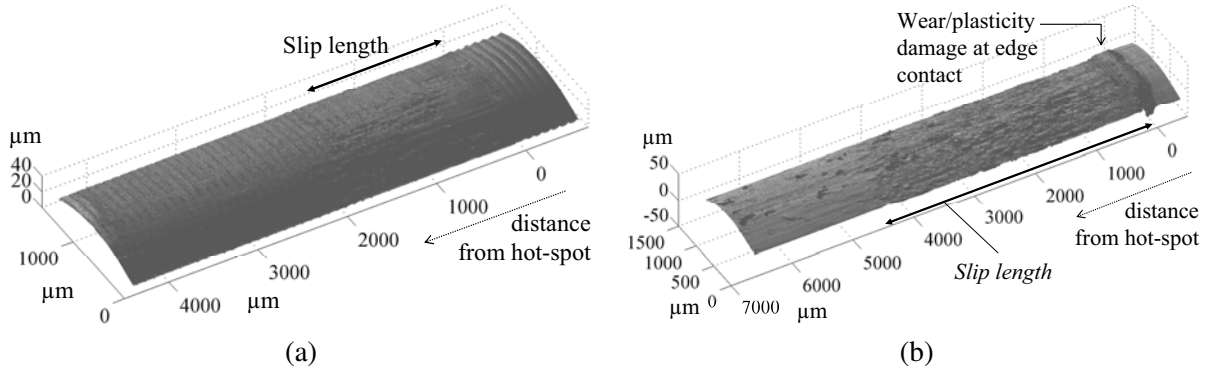

Figure 5: Three-dimensional profile scan for friction evaluation, specimens from: (a) A series, (b) D series.

independent simulations were performed: the preload with an axisymmetric model, and then the bending with an axisymmetric *harmonic* model, Fig. 6. The contact at the fretting interface was imposed as bonded, for the bending model, in order to keep the analysis linear and have the opportunity to use the axisymmetric harmonic element type. The submodel boundary was then placed far enough from the hot-spot in a region where the contact was sticking rather than slipping. The contact interference for the preload simulation was tuned in order to obtain the same strain gage reading as recorded after the shrink-fit. Similarly, the simulated bending load was calculated to match the axial strain gage on the shaft. A coarse mesh was sufficient for these two full models. A submodel was then defined around the position of the fretting hot-spot. This submodel was a plane strain and multiple refinements around the hot-spot produced a 2 µm mesh which was accurate enough for the high gradient contact stresses. The displacements produced by the preload and the bending were interpolated at the lateral sides of the submodel. These displacements were combined and applied to the submodel at different load steps. The first load step was with a preload only, while the following load steps also included incremental bending. The bending displacements were added to those produced by the preload after being multiplied by a fraction ranging from -1 to 1. The single load cycle was divided into 20 load sub-steps, and two bending load cycles were simulated. The first cycle produced some contact irregularity, while the solution was stable from the second cycle thereafter.

3.2. Validation of the FE model

Validations of this numerical procedure were provided in idealized contact conditions which could be compared with just one of the full models. The validation for the shrink-fit load component was obtained with a complete contact, i.e. without the fillet. Initially, the power of singularity was deduced according to Churchman et al. [64] and the singularity was found for the half-plane (aluminium $E = 71.5$ GPa, $\nu = 0.33$) in contact with square wedge (steel $E = 205$ GPa, $\nu = 0.3$) and for different CoF values, Fig. 7 (a). The aluminium-steel elastic parameter combination was found to be in agreement with type A materials according to Churchman's

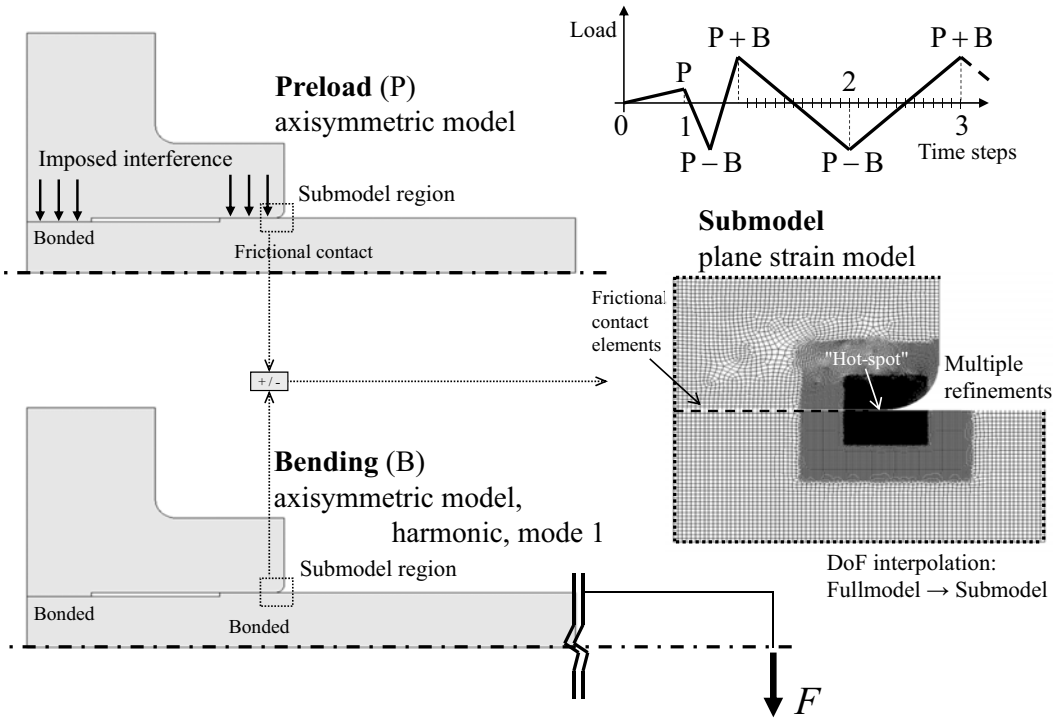

Figure 6: FE modelling, axisymmetric models, load combinations and plane strain submodel.

definition. Thus, as intuitively suggested, if the wedge slips away from the corner, the order of singularity is weaker, while if it slips towards the corner, the stress singularity is exacerbated. According to the present bending loading scheme, the weaker singularity takes place during the tensile half cycle, while the stronger singularity happens during the compressive half cycle. Frictionless contact was modelled for this first validation. The stress singularity with $f = 0$ was retrieved both with a full model and with the submodel featuring a sharp edge contact. The validation was considered successful since the singularity intensities, obtained from the two models, were very similar, Fig. 7 (b). The bending component was then tested under the condition of "infinite" CoF and fillet geometry. Again, the same load was applied to a comparative full model and to the proposed submodel with bonded contact and without any preload. Having reintroduced the contact fillet, and after using the same material for this specific validation case, the local contact edge was crack-like and the square root singularity was expected and obtained, Fig. 8. An accurate match between the submodel and the full reference model was again obtained regarding the singularity stress intensity factor, which was a K_{II} for this case. These two validations, though under specific hypotheses, confirmed the validity of the procedure for both the preload and the bending components.

3.3. Flat and rounded contact stresses

The flat and rounded contact problem can be viewed as the merging of the "inner" and the "outer" (or Hertzian) asymptotes, which define the pressure and the friction traction distributions at the edge of the contact [34, 35,

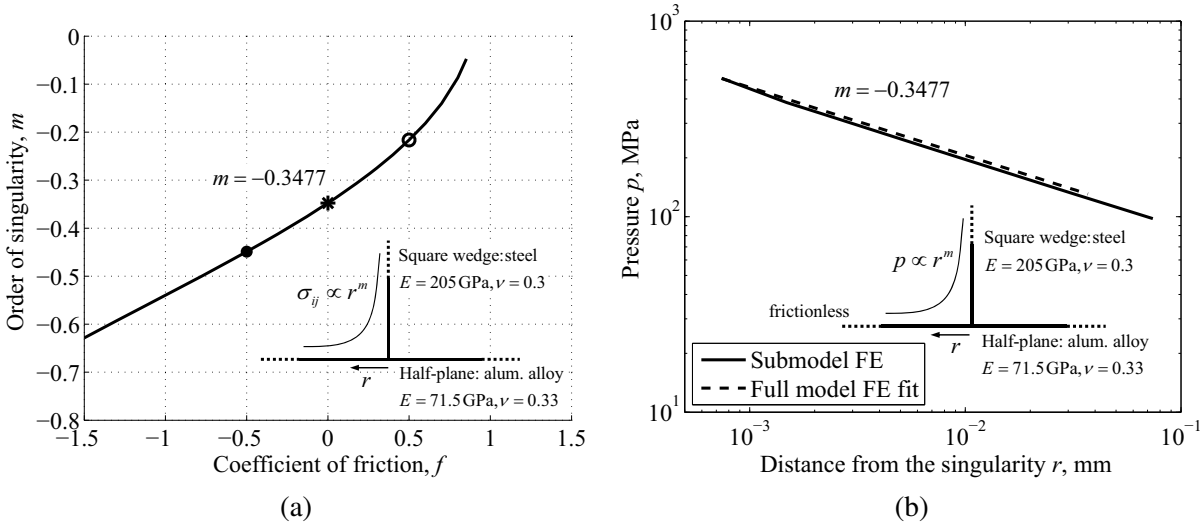

Figure 7: (a) Power of singularity dependence on CoF with half-plane in aluminium and square wedge in steel. (b) FE procedure validation for the shrink-fit preload pressure.

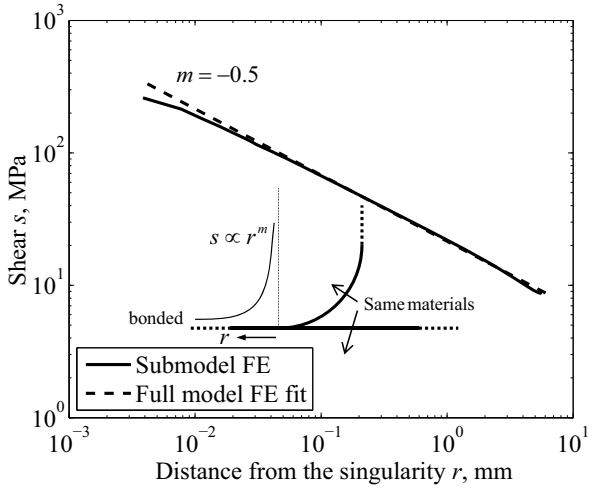

Figure 8: FE procedure validation for the bending shear stress.

40, 42, 65, 66, 67]. Figure 9 shows the numerical results, pressure and shear traction, of the contact near the hot-spot. The high gradient of both the inner and the Hertz asymptotes, along with the vertical derivative of the distribution at the curvature change [68], were well reproduced with the finite element model resolution provided. The contact stresses at the load times $1, 2, 3$ are shown in Figure 6. The initial application of the shrink-fit implies a reversed distribution of the shear. Cyclic bending then generates a slip zone that extends significantly into the flat contact (though not full slip). Therefore, the shear traction around the fretting hot-spot equals the contact pressure times the coefficient of friction. The sign of the shear traction was (conventionally) consistent with the sign of f in Fig. 7 (a): positive for the tensile half cycle and negative for the compressive half cycle. As evident from the graph in Fig. 9, the pressure distribution experiences a cyclic fluctuation. The main reason is the rigidity of the external hub coupled with the aforementioned singularity sensitivity to the friction

traction direction. During the tensile portion the pressure decreases, while it increases during the compressive half cycle. The shear traction reverses from tensile to compressive and also experiences the same fluctuation.

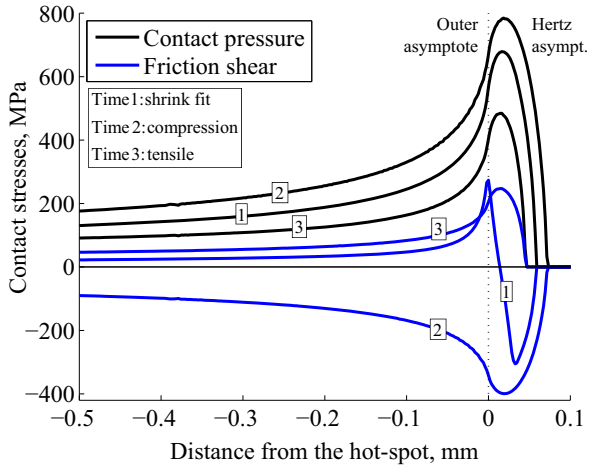

Figure 9: Pressure and shear traction distributions at the fretting cycle time points.

3.4. SIF calculation

The weight function technique was used for calculating the SIFs of the fretting fatigue cracks emanating from the hot-spot. Similar approaches have been followed by Kimura and Sato [69] for the complete contact and Navarro et al. [70] for the Hertzian contact. Beghini et al. [71] proposed a complete weight function formulation for a surface crack, under plane strain and remote boundaries, with a generic crack angle. Though not visible in Fig. 4, the observed fretting cracks featured a strong aspect ratio, i.e. the depth was significantly smaller than the width, thus the plane strain crack configuration was assumed to be accurate. The two plane SIFs, $K_{\mathrm{I}}, K_{\mathrm{II}}$, were obtained as the integration of the normal and shear stresses along the crack line, after having evaluated these stresses without the crack (i.e. the "nominal" stresses). The surface position of the crack line was considered at the point on the specimen side coincident with the flat and rounded tangency on the hub side at the most tensile load history step during the bending cycle. As the crack is at a certain angle, a *coupled* integration was required. When the crack is not perpendicular to the surface, the normal stress affected both mode I and mode II SIFs and, similarly, the shear stress also had an effect on both the two SIFs. The angle for accurate SIF calculation was in the range of -75° to 75° [71] (where the zero angle is the direction perpendicular to the surface line), thus even quite shallow cracks can be considered. Recently, Beghini and Santus [72] applied this weight function formulation to the rolling contact fatigue problem. Similarly, the face contact pressure had to be introduced in the calculation if the crack experienced closure. When the output of the first calculation was negative, $K_{\mathrm{I}} < 0$, the crack face contact distribution was assumed to be proportional to the nominal normal stress. A scaling factor was calculated in order to have $K_{\mathrm{I}} = 0$, and then K_{II} was recalculated. This technique was validated for the

Hertzian rolling contact, with slip, thus including the surface shear traction, with different crack angles. The occurrence of the crack face contact is assumed here to coincide with the condition where $K_I \leq 0$. The crack opening displacement can actually be negative at some point along the crack line (then face contact follows) even for a slightly positive mode I SIF, especially when superimposed to a non-zero mode II loading. However, this effect was not considered in the present analysis since the modelled cracks are only short, thus the entity of the face displacement induced by the load is limited. The weight function technique is also effective for incorporating a residual stress distribution. Based on the superimposition principle, the nominal stresses can be initially calculated with a residual stress free FE model, then the actual residual stress distribution, Fig. 2 (b), can simply be added to the nominal stresses. The fast numerical calculation of the weight function meant that a complete analysis could be made by considering the crack growth evolution along any angle direction either with or without the residual stresses for all the experimental test series.

4. Fretting fatigue prediction

4.1. Fretting crack initiation direction

Observing the direction of the crack is the first step in identifying predictive stress parameters. The experimental evidence reported in Fig. 4 only showed shallow (type I) cracks. These cracks are assumed to be driven by the cyclic shear amplitude, while almost perpendicular (type II) cracks are driven by the normal stress amplitude, without any preliminarily shear based shallow initiation, at least not visible at the micron scale resolution of the SEM [28, 47, 48]. The angle definition followed here is reported in Fig. 10 (a) where the pad position is assumed to be on the left-hand side, the zero angle is for the direction perpendicular to the surface, and the positive sign is counter-clockwise. According to this conventional definition, experimentally observed shallow cracks were at approximately $\alpha = -70°$. The same angle definition was also used for the critical plane orientation, introduced and discussed below, Fig. 10 (b).

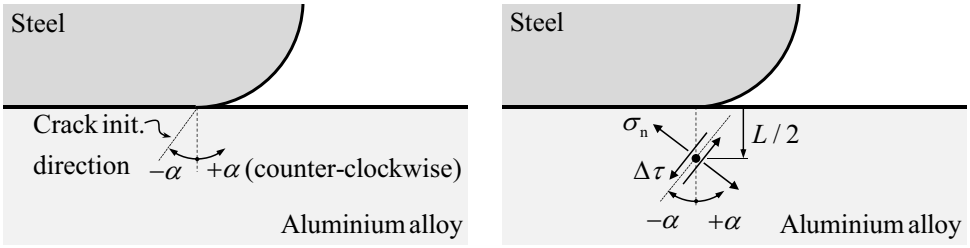

Figure 10: Angular definition, zero for the perpendicular direction and positive counter-clockwise, both for the crack initiation direction (a) and for the critical plane (b).

The initiation crack direction is assessed on the basis of the local stress state during the loading cycle. However,

the multiaxial stress distribution is not evaluated at the surface, especially for the singular complete contact. Usually, the short to long transition crack size on the KT diagram, i.e. the El Haddad length (or Critical Distance) L is considered as an effective size of the process zone, under any fatigue loading, and also for the fretting fatigue [28, 48, 73]. This material length is obtained from the combination of the long crack threshold stress intensity factor range $\Delta K_{\mathrm{th},-1}$ and the axial fatigue limit $\Delta\sigma_{-1}$ or more specifically, the fatigue endurance for aluminium alloys, both evaluated at the load ratio $R=-1$, Eq. 1:

$$L=\frac{1}{\pi}\left(\frac{\Delta K_{\mathrm{th},-1}}{\Delta\sigma_{-1}}\right)^2 \tag{1}$$

The value $L=45$ µm for 7075-T6 alloy was derived from the literature [74], and the stress components for predicting the crack initial direction, and also for the fatigue strength assessment, were evaluated at $L/2$ depth according to the Point Method [20, 46], Fig. 10 (b). The shear stress amplitude τ_{a}, the normal maximum stress $\sigma_{\mathrm{n,max}}$ and the normal stress amplitude $\sigma_{\mathrm{n,a}}$ were calculated for any α angle ranging from -90° to 90° with 1° resolution. These stress components for the A series (without deep rolling) and the D series (with deep rolling) are reported in Fig. 11. B and C series are not reported as the trends were quite similar to A and D respectively.

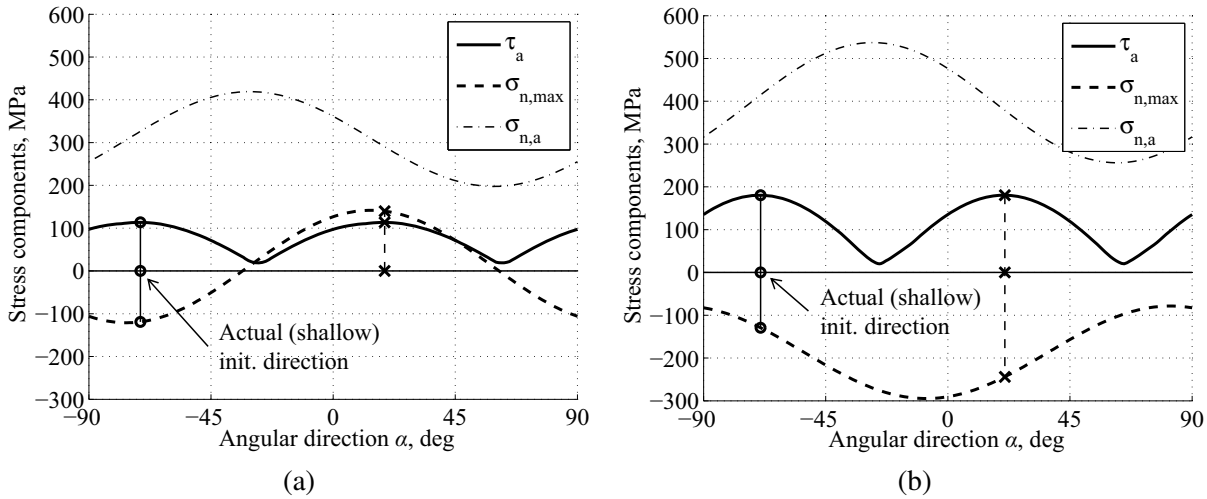

Figure 11: Stress component dependencies on the angle: A series without residual stresses (a), and D series with residual stresses (b).

Giner et al. [28] and Faanes et al. [75] noted that if the maximum shear stress amplitude criterion is followed, due to the stress tensor symmetry, there are two potential directions spaced by an angle of 90° experiencing the same shear stress amplitude. This periodicity of 90° is evident in Fig. 11, and the two maxima has been found one at a very shallow direction toward the pad, at approximately -70°, and the other opposite to the pad and not shallow, at approximately 20°. Since the maximum and minimum values of the normal stress amplitude were almost "out-of-phase" with respect to the shear amplitude, Fig. 11, the two maximum shear planes experienced very similar normal stress amplitudes. Therefore, the crack initiation direction should be identified by the normal

stress $\sigma_{n,max}$ which was quite different between the two maximum shear amplitude planes. The series without residual stresses provided the highest maximum normal stress (tensile) for the positive angle $\alpha = 20°$, while the experimental evidence of the crack was clearly along the other maximum shear amplitude direction. In contrast, the deep rolled series showed the highest maximum normal stress (still compressive) for the negative angle. The introduction of compressive residual stresses, with a principal direction parallel to the surface, introduced the highest contribution near $\alpha = 0°$ and a vanishingly small effect near $\alpha = 90°$ and $\alpha = -90°$. It would seem that the shear amplitude and the normal stress can be effective as initiation criterion for the deep rolled series, but inconsistent for untreated specimens, at least for the present fretting tests.

The SIF ranges were evaluated for potential cracks emanating from the hot-spot with a straight path along different angular directions. Dimensionless SIF ranges are reported for the A series for the two maximum shear stress directions $\alpha = -20°, \alpha = 70°$, Fig. 12. The small crack threshold was evaluated both with the asymptotic model and with the El Haddad equation [43]. The long crack threshold considered $\Delta K_{th,0} = 2.2$ MPa$\sqrt{m}$ [76] was for $R = 0$, which was then compared to the positive portion of the K_I cycle (referred to as $\Delta K_{I,p}$). It is evident that the positive part of the mode I load cycle is not zero only for the positive angle, while the crack remains closed for the shallow crack path. A mode I based criterion for crack initiation again is not consistent, indeed the opposite direction would be identified. It could be conjectured that the mode I SIF has no role in driving the crack at least for the initiation stage. Conversely, ΔK_{II} was found to be higher for the shallow direction than for the positive angle direction, at least for crack sizes comparable to the critical crack length, Fig. 12. The higher ΔK_{II} for the negative angle is due to the coupling effects of the stress components and also to the crack face contact introduced for $\alpha < 0$. If the mode II SIF were related to the shear stress only, these two directions would experience similar ΔK_{II} since they are loaded by the same maximum shear stress amplitude. The deep rolled series always reported $\Delta K_{I,p} = 0$, because of the intensively compressive residual stresses, for any direction of the crack emanating from the hot-spot. As with the untreated series, it was found that ΔK_{II} was higher for the shallow direction. It can be concluded that neither the normal stress nor the mode I SIF are important for identifying the direction of the crack initiation, while the shear stress amplitude along with the mode II SIF range allowed a correct crack angle prediction, both for the untreated and for the deep rolled series. However, this inference should not be considered as general for any fretting contact. The crack paths reported by other researchers usually follow the type II scheme, without the initial shallow path, hence driven by the normal stresses. This particular fretting case can be attributed to the pressure fluctuation. As shown in Fig. 9, the tensile portion of the load cycle is less pronounced than the compressive portion. Under these conditions, the role of the normal stresses is not predominant compared to the shear stresses, which are mainly induced by the friction

traction during the compressive half cycle.

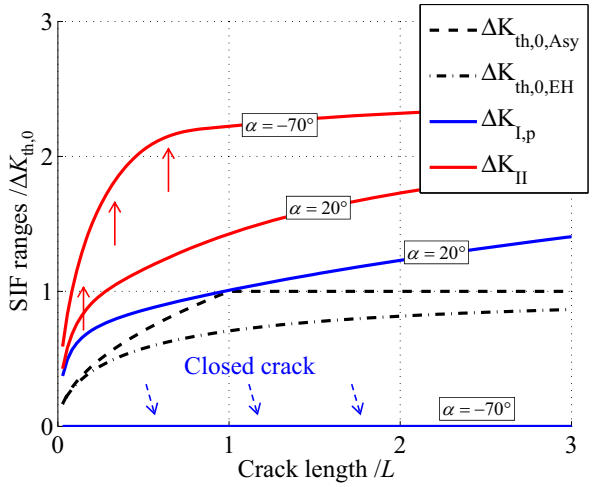

Figure 12: SIF range dependencies on the crack size regarding the A series for maximum shear amplitude directions, $\alpha = 20^\circ$ and $\alpha = -70^\circ$.

4.2. Multiaxial fatigue stress prediction

The availability of the stress distributions, the material properties, and also the direction of the crack initiation, should provide a solid background for predicting the fretting fatigue strength. However, fretting is well known to have particular features such as the stress triaxiality (though a local plane strain can reasonable be assumed), as well as stress non proportionality, stress gradient, friction alteration, and micro-wear and plasticity, all of which that can significantly impair the local actual geometry [77, 78]. As reported in the Introduction, crack arrest and critical plane multiaxial fatigue criterion are some of the most promising approaches [20]. Crack arrest is based on the opening mode I, indeed the fatigue limit is predicted when the small crack threshold and ΔK_{I} are equal for a critical length crack size. Figure 12 reports this condition for test series A, however, this criterion is not effective for the specific fretting tests reported in this paper. The direction of the crack should follow (even approximately) the path angle for which $\Delta K_{\mathrm{I,p}}$ is maximum, or at least positive, while the experimentally observed crack has a 90° misaligned orientation as previously discussed. In addition, the deep rolled specimens always experienced closed cracks, indeed K_{I} was calculated as negative, for any crack angle, after including the deep and highly compressive residual stresses. A critical plane criterion was assumed to be more promising for this set of tests as it is based on the shear stress amplitude rather than mode I crack opening. Different multiaxial fatigue parameters could be considered, both shear based and normal stress based [79]. A combination of the shear stress amplitude τ_{a} and the maximum normal stress $\sigma_{\mathrm{n,max}}$, according to the Modified Wöhler Curve Method, was recently proposed and applied to fretting, Eq. 2 [19, 20, 46]:

$$\tau_{\mathrm{a,eq}} = \tau_{\mathrm{a}} + \kappa \frac{\sigma_{\mathrm{n,max}}}{\tau_{\mathrm{a}}} \tag{2}$$

This equivalent shear stress parameter should then be compared to the torsional fatigue limit λ, and finally an assessment stress ratio can be defined:

$$\eta = \lambda / \tau_{a,eq} \tag{3}$$

Fatigue tests were performed on plain specimens extracted from the same aluminium bars as the fretting shafts, and with the same axial load orientation. Besides the usual load ratio $R = -1$, compressive cycles were also tested, Fig. 13, in order to have a material data spectrum more consistent with the compressive fretting load cycles, especially for the deep rolled series.

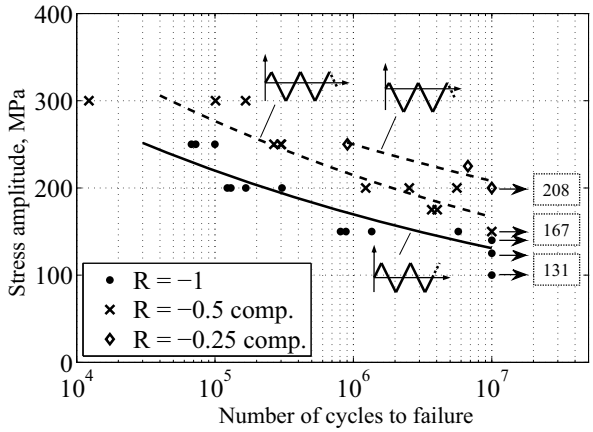

Figure 13: Fatigue results on plain specimens with compressive preponderance load ratios.

After considering these experimental results the κ, λ material properties were derived according to equations reported by Rossino et. al. [19] which combine the reference load ratio $R = -1$ with any other different load ratio. The κ, λ parameters were slightly different for combinations with various R, more specifically the two values were both higher for a more compressive combining load ratio, Tab. 2.

Table 2: Multiaxial fatigue parameters κ, λ as estimated with different load ratio combinations.

$R = -1$ & $R = 0$ (tensile) [1]	$\kappa_1 = 12$ MPa, $\lambda_1 = 78$ MPa
$R = -1$ & $R = -0.5$ (compressive)	$\kappa_2 = 54$ MPa, $\lambda_2 = 120$ MPa
$R = -1$ & $R = -0.25$ (compressive)	$\kappa_3 = 64$ MPa, $\lambda_3 = 130$ MPa

The material critical distance at $R = -1$ was assumed as $L = 45$ µm according to the literature as reported above. However, if Eq. 1 is applied with the long crack threshold $\Delta K_{th,-1} = 4.0\ \text{MPa}\sqrt{\text{m}}$ [76] and the $R = -1$ fatigue limit amplitude reported in Fig. 13, a slightly larger El Haddad length follows: $L = 74$ µm. Another uncertainty is the angular α to be considered for series A and B for which the crack direction did not match the most detrimental $\sigma_{n,max}$ of the two maximum τ_a orientations. This was not the case for the two deep rolled

[1] The $R = 0$ tensile fatigue limit was estimated by the Goodman model.

series for which the shallow crack angle was in agreement with the worst stress combination, as discussed above. The uncertainties regarding the angular orientation for the untreated series A and B, the actual value of the material length L, and the material parameters κ, λ are all included in the results reported in Table 3. The fretting fatigue assessment can be considered as satisfactory given that the η values obtained are near to unity. However, the main concern regards the discrimination between untreated vs. deep rolled series. If the maximum τ_a angle in agreement with the crack observation is chosen (the first column in Table 3), different κ, λ material parameters should be taken into account, considering the different compressive predominance, otherwise the more detrimental shear stress amplitude for the deep rolled series, Fig. 11, is not recovered by the normal stress which is almost the same for the shallow directions. Alternatively, a reasonable assessment is again obtained if the most detrimental angle is considered for the A and B series, without taking into account whether or not it is in agreement the crack direction. Indeed, the second column in Table 3 shows positive α angles that experienced higher maximum normal stresses for the untreated series A and B, which were then recovered by the compressive residual stresses for series C and D. Finally, the effect of a larger L implied lower point method stresses and higher λ ratios. However, this issue was more pertinent for series C and D, for which a deep compressive region was induced by the treatment.

Table 3: Assessment stress ratio $\eta = \lambda / \tau_{a,eq}$ results after different assumptions.

Series	$L = 45$ μm	$L = 45$ μm	$L = 74$ μm
A	$\eta = 0.77$ ($\alpha = -71°, \kappa_1\lambda_1$)	$\eta = 0.67$ ($\alpha = 19°, \kappa_2\lambda_2$)	$\eta = 0.72$ ($\alpha = 11°, \kappa_2\lambda_2$)
B	$\eta = 0.87$ ($\alpha = -77°, \kappa_1\lambda_1$)	$\eta = 0.66$ ($\alpha = 13°, \kappa_2\lambda_2$)	$\eta = 0.72$ ($\alpha = 11°, \kappa_2\lambda_2$)
C	$\eta = 0.96$ ($\alpha = -70°, \kappa_3\lambda_3$)	$\eta = 0.85$ ($\alpha = -70°, \kappa_2\lambda_2$)	$\eta = 1.61$ ($\alpha = -69°, \kappa_2\lambda_2$)
D	$\eta = 0.97$ ($\alpha = -69°, \kappa_3\lambda_3$)	$\eta = 0.85$ ($\alpha = -69°, \kappa_2\lambda_2$)	$\eta = 1.64$ ($\alpha = -71°, \kappa_2\lambda_2$)

5. Conclusions

The paper proposes a new configuration for fretting fatigue testing featuring a round geometry, which prevents any misalignment and edge effect, and with fatigue loading applied as bending. This test configuration was used for a comparative analysis regarding the effects of lubrication and deep rolling treatment. The main conclusions of this study are:

- The reduced coefficient of friction enhanced the fretting fatigue, especially for the non rolled specimens that experienced a lower cyclic bending load and consequently lubrication was maintained.
- Deep rolling produced a significant fretting fatigue enhancement in terms of bending load. This strength increase was attributed to the introduction of the residual stresses, from the modelling point of view, while other effects also play a role, such as the hardness enhancement and/or the surface finish improvement.

- A finite element model was implemented and validated, and the stress calculation was solved as three step plane models, without any cumbersome 3D modelling, obtaining very accurate pressure and shear distributions.
- SEM observations reported multiple cracks with branching or coalescence in some cases. The early stage crack direction was always shallow and toward the inside of the contact.
- This shallow direction was in agreement with one direction of maximum shear stress amplitude, however, untreated specimens had the most detrimental direction toward the outside of the contact.
- The mode II stress intensity factor range enabled the correct initiation direction to be identified, for the untreated specimens. Indeed, of the two highest shear stress amplitude directions, that aligned with the actual crack experienced the highest mode II SIF range.
- A multiaxial stress fatigue criterion was applied for both untreated and deep rolled series. Although some uncertainties regarding the material properties and again the angle to be considered, the assessment ratio was found to be near unity.
- The crack arrest was not considered to be adequate for this specific testing configuration, where the shear stress amplitude was more predominant than the tensile load. This was due to the deep rolling compressive stresses or, for the untreated specimens, to the pressure fluctuation during the bending cycle. This would seem to be a drawback of the proposed test setup, however, it offers a specific fretting configuration that is usual for the shrink-fit shafts and tubular connections.

Acknowledgments

This work was carried out as part of the Italian research program PRIN 2009Z55NWC. The authors would like to express their gratitude for the funding.

References

[1] P. McVeigh, G. Harish, T. Farris, M. Szolwinski, Modeling interfacial conditions in nominally flat contacts for application to fretting fatigue of turbine engine components, International Journal of Fatigue 21 (Suppl. 1) (1999) S157–S165.
[2] B. Carter, E. Schenck, P. Wawrzynek, A. Ingraffea, K. Barlow, Three-dimensional simulation of fretting crack nucleation and growth, Engineering Fracture Mechanics 96 (2012) 447–460, DOI: 10.1016/j.engfracmech.2012.08.015.
[3] K. Chan, M. Enright, J. Moody, P. Golden, R. Chandra, A. Pentz, Residual stress profiles for mitigating fretting fatigue in gas turbine engine disks, International Journal of Fatigue 32 (5) (2010) 815–823, DOI: 10.1016/j.ijfatigue.2009.07.004.
[4] P. Golden, J. Calcaterra, A fracture mechanics life prediction methodology applied to dovetail fretting, Tribology International 39 (10) (2006) 1172–1180, DOI: 10.1016/j.triboint.2006.02.006.
[5] T. Juuma, Torsional fretting fatigue strength of a shrink-fitted shaft, Wear 231 (2) (1999) 310–318, DOI: 10.1016/S0043-1648(99)00249-5.
[6] T. Juuma, Torsional fretting fatigue strength of a shrink-fitted shaft with a grooved hub, Tribology International 33 (8) (2000) 537–543, DOI: 10.1016/S0301-679X(00)00102-X.

[7] C. Santus, L. Bertini, M. Beghini, Fretting fatigue apparatus for shrink-fitted shaft assembly, Applied Mechanics and Materials 7-8 (2007) 43–48, DOI: 10.4028/www.scientific.net/AMM.7-8.43.
[8] C. Santus, Fretting fatigue of aluminum alloy in contact with steel in oil drill pipe connections, modeling to interpret test results, International Journal of Fatigue 30 (4) (2008) 677–688, DOI: 10.1016/j.ijfatigue.2007.05.006.
[9] L. Bertini, M. Beghini, C. Santus, A. Baryshnikov, Resonant test rigs for fatigue full scale testing of oil drill string connections, International Journal of Fatigue 30 (6) (2008) 978–988, DOI: 10.1016/j.ijfatigue.2007.08.013.
[10] B. Alfredsson, Fretting fatigue of a shrink-fit pin subjected to rotating bending: Experiments and simulations, International Journal of Fatigue 31 (10) (2009) 1559–1570, DOI: 10.1016/j.ijfatigue.2009.04.019.
[11] E. Leidich, J. Vidner, B. Brůžek, Integral Approach for Endurance Limit Evaluation on Shrink-Fitted Assemblies, Bulletin of Applied Mechanics 5 (18) (2009) 44–49.
[12] D. Hills, D. Nowell, Mechanics of Fretting Fatigue, Kluwer Academic Publishers, 1994, ISBN 0-7923-2866-3.
[13] J. D. Pauw, P. D. Baets, W. D. Waele, Review and classification of fretting fatigue test rigs, Sustainable Construction and Design 2 (1) (2011) 41–52.
[14] P. Golden, M. Shepard, Life prediction of fretting fatigue with advanced surface treatments, Materials Science and Engineering A 468-470 (Special Issue) (2007) 15–22, DOI: 10.1016/j.msea.2006.10.168.
[15] C. Azevedo, A. Henriques, A. P. Filho, J. Ferreira, J. Araújo, Fretting fatigue in overhead conductors: Rig design and failure analysis of a grosbeak aluminium cable steel reinforced conductor, Engineering Failure Analysis 16 (1) (2009) 136–151, DOI: 10.1016/j.engfailanal.2008.01.003.
[16] M. Attia, R. Waterhouse, Standardization of Fretting Fatigue Test Methods and Equipments, ASTM, 1992, STP 1159.
[17] D. Hoeppner, V. Chandrasekaran, C. Elliott III, Fretting Fatigue: Current Technology and Practices, ASTM, 2000, STP 1367.
[18] Y. Mutoh, D. Hoeppner, S. Kinyon, Fretting Fatigue: Advances in Basic Understanding and Applications, ASTM, 2003, STP 1425.
[19] L. Rossino, F. Castro, W. B. Filho, J. Araújo, Issues on the mean stress effect in fretting fatigue of a 7050-T7451 Al alloy posed by new experimental data, International Journal of Fatigue 31 (11-12) (2009) 2041–2048, DOI: 10.1016/j.ijfatigue.2008.12.011.
[20] J. Araújo, F. Castro, A comparative analysis between multiaxial stress and ΔK-based short crack arrest models in fretting fatigue, Engineering Fracture Mechanics 93 (2012) 34–47, DOI: 10.1016/j.engfracmech.2012.06.007.
[21] C. Lykins, S. Mall, V. Jain, Evaluation of parameters for predicting fretting fatigue crack initiation, International Journal of Fatigue 22 (8) (2000) 703–716, DOI: 10.1016/S0142-1123(00)00036-0.
[22] C. Lykins, S. Mall, V. Jain, A shear stress-based parameter for fretting fatigue crack initiation, Fatigue and Fracture of Engineering Materials and Structures 24 (7) (2001) 461–473, DOI: 10.1046/j.1460-2695.2001.00412.x.
[23] M. Szolwinski, T. Farris, Observation, analysis and prediction of fretting fatigue in 2024-T351 aluminum alloy, Wear 221 (1) (1998) 24–36, DOI: 10.1016/S0043-1648(98)00264-6.
[24] S. Muñoz, H. Proudhon, J. Domínguez, S. Fouvry, Prediction of the crack extension under fretting wear loading conditions, International Journal of Fatigue 28 (12) (2006) 1769–1779, DOI: 10.1016/j.ijfatigue.2006.01.002.
[25] D. Swalla, R. Neu, Influence of coefficient of friction on fretting fatigue crack nucleation prediction, Tribology International 34 (7) (2001) 493–503, DOI: 10.1016/S0301-679X(01)00048-2.
[26] B. Wittkowsky, P. Birch, J. Dominguez, S. Suresh, Apparatus for quantitative fretting fatigue testing, Fatigue and Fracture of Engineering Materials and Structures 22 (4) (1999) 307–320, DOI: 10.1046/j.1460-2695.1999.00145.x.
[27] R. Hojjati-Talemi, M. Wahab, E. Giner, M. Sabsabi, Numerical estimation of fretting fatigue lifetime using damage and fracture mechanics, Tribology Letters 52 (1) (2013) 11–25, DOI: 10.1007/s11249-013-0189-8.
[28] E. Giner, M. Sabsabi, J. Ródenas, F. J. Fuenmayor, Direction of crack propagation in a complete contact fretting-fatigue problem, International Journal of Fatigue 58 (2014) 172–180, DOI: 10.1016/j.ijfatigue.2013.03.001.
[29] N. Noraphaiphipaksa, C. Kanchanomai, Y. Mutoh, Numerical and experimental investigations on fretting fatigue: Relative slip, crack path, and fatigue life, Engineering Fracture Mechanics 112-113 (2013) 58–71, DOI: 10.1016/j.engfracmech.2013.10.007.
[30] S. Namjoshi, S. Mall, V. Jain, O. Jin, Fretting fatigue crack initiation mechanism in Ti-6Al-4V, Fatigue and Fracture of Engineering Materials and Structures 25 (10) (2002) 955–964, DOI: 10.1046/j.1460-2695.2002.00549.x.
[31] H. Kim, S. Mall, Investigation into three-dimensional effects of finite contact width on fretting fatigue, Finite Elements in Analysis and Design 41 (11-12) (2005) 1140–1159, DOI: 10.1016/j.finel.2005.02.001.
[32] K. Liu, M. Hill, The effects of laser peening and shot peening on fretting fatigue in Ti-6Al-4V coupons, Tribology International 42 (9) (2009) 1250–1262, DOI: 10.1016/j.triboint.2009.04.005.
[33] D. Hills, R. Flicek, A discussion of "Numerical and experimental investigations on fretting fatigue: Relative slip, crack path, and fatigue life" by N. Noraphaiphipaksa, C. Kanchanomai, and Y. Mutoh, Engineering Fracture Mechanics 133 (2015) 52–55, DOI: 10.1016/j.engfracmech.2014.10.024.
[34] D. Nowell, D. Dini, D. Hills, Recent developments in the understanding of fretting fatigue, Engineering Fracture Mechanics 73 (2) (2006) 207–222, DOI: 10.1016/j.engfracmech.2005.01.013.
[35] D. Hills, A. Thaitirarot, J. Barber, D. Dini, Correlation of fretting fatigue experimental results using an asymptotic approach, International Journal of Fatigue 43 (2012) 62–75, DOI: 10.1016/j.ijfatigue.2012.02.006.
[36] M. Ciavarella, A 'crack-like' notch analogue for a safe-life fretting fatigue design methodology, Fatigue and Fracture of Engineering Materials and Structures 26 (12) (2003) 1159–1170, DOI: 10.1046/j.1460-2695.2003.00721.x.
[37] M. Ciavarella, D. Dini, A refined clna model in fretting fatigue using asymptotic characterization of the contact stress fields, Fatigue and Fracture of Engineering Materials and Structures 28 (12) (2005) 1099–1112, DOI: 10.1111/j.1460-2695.2005.00948.x.
[38] M. Ciavarella, Some observations on the clna model in fretting fatigue, Tribology International 39 (10) (2006) 1142–1148, DOI: 10.1016/j.triboint.2006.02.032.

[39] S. Naboulsi, Applications of crack analogy to fretting fatigue, Engineering Fracture Mechanics 72 (10) (2005) 1610–1623, DOI: 10.1016/j.engfracmech.2004.11.006.
[40] D. Hills, D. Dini, A new method for the quantification of nucleation of fretting fatigue cracks using asymptotic contact solutions, Tribology International 39 (10) (2006) 1114–1122, DOI: 10.1016/j.triboint.2006.02.041.
[41] D. Hills, R. Flicek, D. Dini, A discussion of: Development of a complete contact fretting test device by J Juoksukangas et al., Proceedings of the Institution of Mechanical Engineers, Part J: Journal of Engineering Tribology 228 (1) (2014) 123–126, DOI: 10.1177/1350650113500946.
[42] D. Dini, D. Hills, Bounded asymptotic solutions for incomplete contacts in partial slip, International Journal of Solids and Structures 41 (24-25) (2004) 7049–7062, DOI: 10.1016/j.ijsolstr.2004.05.058.
[43] D. Dini, D. Nowell, I. Dyson, The use of notch and short crack approaches to fretting fatigue threshold prediction: Theory and experimental validation, Tribology International 39 (10) (2006) 1158–1165, DOI: 10.1016/j.triboint.2006.02.033.
[44] J. Araújo, D. Nowell, Analysis of pad size effects in fretting fatigue using short crack arrest methodologies, International Journal of Fatigue 21 (9) (1999) 947–956, DOI: 10.1016/S0142-1123(99)00077-8.
[45] C. Vallellano, J. Dominguez, A. Navarro, On the estimation of fatigue failure under fretting conditions using notch methodologies, Fatigue and Fracture of Engineering Materials and Structures 26 (5) (2003) 469–478, DOI: 10.1046/j.1460-2695.2003.00649.x.
[46] J. Araújo, L. Susmel, D. Taylor, J. Ferro, E. Mamiya, On the use of the Theory of Critical Distances and the Modified Wöhler Curve Method to estimate fretting fatigue strength of cylindrical contacts, International Journal of Fatigue 29 (1) (2007) 95–107, DOI: 10.1016/j.ijfatigue.2006.02.041.
[47] V. Lamacq, M.-C. Dubourg, Modelling of initial fatigue crack growth and crack branching under fretting conditions, Fatigue and Fracture of Engineering Materials and Structures 22 (6) (1999) 535–542, DOI: 10.1046/j.1460-2695.1999.00173.x.
[48] Y. Mutoh, J.-Q. Xu, Fracture mechanics approach to fretting fatigue and problems to be solved, Tribology International 36 (2) (2003) 99–107, DOI: 10.1016/S0301-679X(02)00136-6.
[49] J. Juoksukangas, A. Lehtovaara, A. Mäntylä, Development of a complete contact fretting test device, Proceedings of the Institution of Mechanical Engineers, Part J: Journal of Engineering Tribology 227 (6) (2013) 570–578, DOI: 10.1177/1350650112466162.
[50] M. Benedetti, V. Fontanari, P. Scardi, C. Ricardo, M. Bandini, Reverse bending fatigue of shot peened 7075–T651 aluminium alloy: The role of residual stress relaxation, International Journal of Fatigue 31 (8-9) (2009) 1225–1236, DOI: 10.1016/j.ijfatigue.2008.11.017.
[51] P. Prevéy, J. Cammett, The influence of surface enhancement by low plasticity burnishing on the corrosion fatigue performance of AA7075-T6, International Journal of Fatigue 26 (9) (2004) 975–982, DOI: 10.1016/j.ijfatigue.2004.01.010.
[52] S. H-Gangaraj, Y. Alvandi-Tabrizi, G. Farrahi, G. Majzoobi, H. Ghadbeigi, Finite element analysis of shot-peening effect on fretting fatigue parameters, Tribology International 44 (11) (2011) 1583–1588, DOI: 10.1016/j.triboint.2010.11.023.
[53] G. Majzoobi, K. Azadikhah, J. Nemati, The effects of deep rolling and shot peening on fretting fatigue resistance of Aluminum-7075-T6, Materials Science and Engineering A 516 (1-2) (2009) 235–247, DOI: 10.1016/j.msea.2009.03.020.
[54] G. Majzoobi, A. Ahmadkhani, The effects of multiple re-shot peening on fretting fatigue behavior of Al7075-T6, Surface and Coatings Technology 205 (1) (2010) 102–109, DOI: 10.1016/j.surfcoat.2010.06.014.
[55] M. Beghini, L. Bertini, B. Monelli, C. Santus, M. Bandini, Experimental parameter sensitivity analysis of residual stresses induced by deep rolling on 7075-T6 aluminium alloy, Surface and Coatings Technology 254 (2014) 175–186, DOI: 10.1016/j.surfcoat.2014.06.008.
[56] M. Benedetti, V. Fontanari, C. Santus, M. Bandini, Notch fatigue behaviour of shot peened high-strength aluminium alloys: Experiments and predictions using a critical distance method, International Journal of Fatigue 32 (10) (2010) 1600–1611, DOI: 10.1016/j.ijfatigue.2010.02.012.
[57] S. Fouvry, V. Fridrici, C. Langlade, P. Kapsa, L. Vincent, Palliatives in fretting: A dynamical approach, Tribology International 39 (10) (2006) 1005–1015, DOI: 10.1016/j.triboint.2006.02.038.
[58] S. Suresh, Fatigue of Materials, Cambridge University Press, 2004, ISBN: 978-0-521-57046-6.
[59] T. Lindley, Fretting fatigue in engineering alloys, International Journal of Fatigue 19 (Soppl.1) (1997) S39–S49.
[60] Z. Zhou, L. Vincent, Lubrication in fretting – a review, Wear 225-229 (PART II) (1999) 962–967.
[61] J. D. Pauw, W. D. Waele, R. Hojjati-Talemi, P. D. Baets, On the use of digital image correlation for slip measurement during coupon scale fretting fatigue experiments, International Journal of Solids and Structures 51 (18) (2014) 3058–3066, DOI: 10.1016/j.ijsolstr.2014.05.002.
[62] R. Hojjati-Talemi, M. A. Wahab, J. D. Pauw, P. D. Baets, Prediction of fretting fatigue crack initiation and propagation lifetime for cylindrical contact configuration, Tribology International 76 (2014) 73–91, DOI: 10.1016/j.triboint.2014.02.017.
[63] C. Santus, L. Bertini, M. Beghini, A. Merlo, A. Baryshnikov, Torsional strength comparison between two assembling techniques for aluminium drill pipe to steel tool joint connection, International Journal of Pressure Vessels and Piping 86 (2-3) (2009) 177–186, DOI: 10.1016/j.ijpvp.2008.09.007.
[64] C. Churchman, A. Mugadu, D. Hills, Asymptotic results for slipping complete frictional contacts, European Journal of Mechanics, A/Solids 22 (6) (2003) 793–800, DOI: 10.1016/S0997-7538(03)00074-3.
[65] A. Sackfield, A. Mugadu, J. Barber, D. Hills, The application of asymptotic solutions to characterising the process zone in almost complete frictionless contacts, Journal of the Mechanics and Physics of Solids 51 (7) (2003) 1333–1346, DOI: 10.1016/S0022-5096(03)00020-6.
[66] D. Dini, A. Sackfield, D. Hills, Comprehensive bounded asymptotic solutions for incomplete contacts in partial slip, Journal of the Mechanics and Physics of Solids 53 (2) (2005) 437–454, DOI: 10.1016/j.jmps.2004.06.011.
[67] A. Mugadu, D. Hills, J. Barber, A. Sackfield, The application of asymptotic solutions to characterising the process

zone in almost complete frictional contacts, International Journal of Solids and Structures 41 (2) (2004) 385–397, DOI: 10.1016/j.ijsolstr.2003.09.038.
[68] M. Beghini, C. Santus, Analysis of the contact between cubic profiles, International Journal of Mechanical Sciences 46 (2004) 609–621, DOI: 10.1016/j.ijmecsci.2004.05.001.
[69] T. Kimura, K. Sato, Simplified method to determine contact stress distribution and stress intensity factors in fretting fatigue, International Journal of Fatigue 25 (7) (2003) 633–640, DOI: 10.1016/S0142-1123(02)00176-7.
[70] C. Navarro and S. Muñoz and J. Domínguez, Propagation in fretting fatigue from a surface defect, Tribology International 39 (10) (2006) 1149–1157, DOI: 10.1016/j.triboint.2006.02.004.
[71] M. Beghini, L. Bertini, V. Fontanari, Weight function for an inclined edge crack in a semiplane, International Journal of Fracture 99 (4) (1999) 281–292.
[72] M. Beghini, C. Santus, An application of the weight function technique to inclined surface cracks under rolling contact fatigue, assessment and parametric analysis, Engineering Fracture Mechanics 98 (1) (2013) 153–168, DOI: 10.1016/j.engfracmech.2012.10.024.
[73] E. Giner, N. Sukumar, F. Denia, F. Fuenmayor, Extended finite element method for fretting fatigue crack propagation, International Journal of Solids and Structures 45 (22-23) (2008) 5675–5687, DOI: 10.1016/j.ijsolstr.2008.06.009.
[74] C. Santus, D. Taylor, Physically short crack propagation in metals during high cycle fatigue, International Journal of Fatigue 31 (8-9) (2009) 1356–1365, DOI: 10.1016/j.ijfatigue.2009.03.002.
[75] S. Faanes, Inclined cracks in fretting fatigue, Engineering Fracture Mechanics 52 (1) (1995) 71–82.
[76] D. Kujawski, A fatigue crack driving force parameter with load ratio effects, International Journal of Fatigue 23 (SUPPL.1) (2001) S239–S246.
[77] T. Hattori, T. Watanabe, Fretting fatigue strength estimation considering the fretting wear process, Tribology International 39 (10) (2006) 1100–1105, DOI: 10.1016/j.triboint.2006.02.049.
[78] L. Bohórquez, J. Domínguez, Elastic-plastic analysis of a punch and its equivalent notch under fretting conditions, International Journal of Mechanical Sciences 66 (2013) 120–131, DOI: 10.1016/j.ijmecsci.2012.10.013.
[79] J. Araújo, D. Nowell, The effect of rapidly varying contact stress fields on fretting fatigue, International Journal of Fatigue 24 (7) (2002) 763–775, DOI: 10.1016/S0142-1123(01)00191-8.